

NASA/TM—2014-218365



Properties of Desert Sand and CMAS Glass

Narottam P. Bansal
Glenn Research Center, Cleveland, Ohio

Sung R. Choi
Naval Air Systems Command, Patuxent River, Maryland

NASA STI Program . . . in Profile

Since its founding, NASA has been dedicated to the advancement of aeronautics and space science. The NASA Scientific and Technical Information (STI) program plays a key part in helping NASA maintain this important role.

The NASA STI Program operates under the auspices of the Agency Chief Information Officer. It collects, organizes, provides for archiving, and disseminates NASA's STI. The NASA STI program provides access to the NASA Aeronautics and Space Database and its public interface, the NASA Technical Reports Server, thus providing one of the largest collections of aeronautical and space science STI in the world. Results are published in both non-NASA channels and by NASA in the NASA STI Report Series, which includes the following report types:

- **TECHNICAL PUBLICATION.** Reports of completed research or a major significant phase of research that present the results of NASA programs and include extensive data or theoretical analysis. Includes compilations of significant scientific and technical data and information deemed to be of continuing reference value. NASA counterpart of peer-reviewed formal professional papers but has less stringent limitations on manuscript length and extent of graphic presentations.
- **TECHNICAL MEMORANDUM.** Scientific and technical findings that are preliminary or of specialized interest, e.g., quick release reports, working papers, and bibliographies that contain minimal annotation. Does not contain extensive analysis.
- **CONTRACTOR REPORT.** Scientific and technical findings by NASA-sponsored contractors and grantees.

- **CONFERENCE PUBLICATION.** Collected papers from scientific and technical conferences, symposia, seminars, or other meetings sponsored or cosponsored by NASA.
- **SPECIAL PUBLICATION.** Scientific, technical, or historical information from NASA programs, projects, and missions, often concerned with subjects having substantial public interest.
- **TECHNICAL TRANSLATION.** English-language translations of foreign scientific and technical material pertinent to NASA's mission.

Specialized services also include creating custom thesauri, building customized databases, organizing and publishing research results.

For more information about the NASA STI program, see the following:

- Access the NASA STI program home page at <http://www.sti.nasa.gov>
- E-mail your question to help@sti.nasa.gov
- Fax your question to the NASA STI Information Desk at 443-757-5803
- Phone the NASA STI Information Desk at 443-757-5802
- Write to:
STI Information Desk
NASA Center for AeroSpace Information
7115 Standard Drive
Hanover, MD 21076-1320

NASA/TM—2014-218365



Properties of Desert Sand and CMAS Glass

Narottam P. Bansal
Glenn Research Center, Cleveland, Ohio

Sung R. Choi
Naval Air Systems Command, Patuxent River, Maryland

National Aeronautics and
Space Administration

Glenn Research Center
Cleveland, Ohio 44135

August 2014

Acknowledgments

Desert sand was supplied by NAVAIR. Thanks are due to Dr. Paul Angel, Dr. Richard Rogers, Dr. Valerie Wiesner, Doug Doza, Ralph Pawlik, Derek Johnson, Bob Angus, and Ray Babuder for technical assistance during this work. This research was supported by NASA's Aeronautical Sciences Project as well as by NAVAIR through a space act agreement (SAA3-1260).

Level of Review: This material has been technically reviewed by technical management.

Available from

NASA Center for Aerospace Information
7115 Standard Drive
Hanover, MD 21076-1320

National Technical Information Service
5301 Shawnee Road
Alexandria, VA 22312

Available electronically at <http://www.sti.nasa.gov>

Properties of Desert Sand and CMAS Glass

Narottam P. Bansal
National Aeronautics and Space Administration
Glenn Research Center
Cleveland, Ohio 44135

Sung R. Choi
Naval Air Systems Command
Patuxent River, Maryland 20670

Abstract

As-received desert sand from a Middle East country has been characterized for its phase composition and thermal stability. X-ray diffraction analysis showed the presence of quartz (SiO_2), calcite (CaCO_3), gypsum ($\text{CaSO}_4 \cdot 2\text{H}_2\text{O}$), and $\text{NaAlSi}_3\text{O}_8$ phases in as-received desert sand and showed weight loss of ~35 percent due to decomposition of CaCO_3 and $\text{CaSO}_4 \cdot 2\text{H}_2\text{O}$ when heated to 1400 °C. A batch of as-received desert sand was melted into calcium magnesium aluminosilicate (CMAS) glass at ~1500 °C. From inductively coupled plasma-atomic emission spectrometry, chemical composition of the CMAS glass was analyzed to be 27.8CaO-4MgO-5Al₂O₃-61.6SiO₂-0.6Fe₂O₃-1K₂O (mole %). Various physical, thermal and mechanical properties of the glass have been evaluated. Bulk density of CMAS glass was 2.69 g/cm³, Young's modulus 92 GPa, Shear modulus 36 GPa, Poisson's ratio 0.28, dilatometric glass transition temperature (T_g) 706 °C, softening point (T_d) 764 °C, Vickers microhardness 6.3±0.4 GPa, indentation fracture toughness 0.75±0.15 MPa.m^{1/2}, and coefficient of thermal expansion (CTE) 9.8×10⁻⁶/°C in the temperature range 25 to 700 °C. Temperature dependence of viscosity has also been estimated from various reference points of the CMAS glass using the Vogel-Fulcher-Tamman (VFT) equation. The glass remained amorphous after heat treating at 850 °C for 10 hr but crystallized into CaSiO₃ and Ca-Mg-Al silicate phases at 900 °C or higher temperatures. Crystallization kinetics of the CMAS glass has also been investigated by differential thermal analysis (DTA). Activation energies for the crystallization of two different phases in the glass were calculated to be 403 and 483 kJ/mol, respectively.

1.0 Introduction

Ingested particulate materials such as sand, fly ash, and volcanic ash may cause serious damage by erosion as it passes through the jet engine or by plugging the cooling holes of the combustor liner and the blades resulting in premature failure. To improve efficiency, future jet engines will operate at much higher temperatures than the current engines. At these elevated operating temperatures, desert sand or runway dust ingested into turbine engines will melt into a viscous and corrosive slag-like material of calcium magnesium aluminosilicate (CMAS) composition. Sand and molten CMAS may chemically interact and/or infiltrate into the pores of thermal and environmental barrier coatings (TBC/EBC) and may deposit on the surfaces of various engine components (Refs. 1 to 6). These processes could adversely affect the performance and life of jet engines. To help understand the effects of CMAS on durability and life of TBCs and EBCs, it would be beneficial if various properties of the desert sand glass are available.

The objective of the current study was to characterize the as-received desert sand from a Middle East country for its composition and thermal stability and also to evaluate the various physical, thermal, and mechanical properties of the CMAS glass resulting from melting of the desert sand.

2.0 Experimental Methods

2.1 Glass Melting

Desert sand from a Middle East country was melted into glass in a Pt crucible using a programmable box furnace. As-received sand was heated at a rate of 10 °C/minute with isothermal holds of 30 min each at 150, 790, and 1275 °C. After holding at 1500 °C for about an hour for homogenization of the melt, it was quenched in water. The resulting glass frit was ground to powder in a Fritsch Planetary Mill (Model# LC 106-A) using corundum grinding bowl and zirconia milling media.

2.2 Chemical Analysis

Chemical composition of the glass powder was analyzed by inductively coupled plasma-atomic emission spectrometry (ICP-AES) using a Varian Vista Pro model in the axial configuration. About 100 mg of glass powder was fused with 1 g of sodium carbonate to convert it into soluble form. A reagent blank was carried through the procedure to subtract out impurities from sodium carbonate, particularly the alkali metals. A qualitative scan was done to determine the major and minor constituents. This was followed by a quantitative analysis by comparison with standards of known concentration to create calibration curves for each of the desired elements.

2.3 Hot Pressing

The glass powder was loaded into a graphite die and hot pressed in vacuum at ~800 °C under 17 MPa (2.5 ksi) for 10 to 15 min into discs and bars using a Centorr mini hot press. The applied pressure was released before onset of cooling. Grafoil was used as spacers between the samples and the punches.

Surfaces of hot pressed samples were ground and polished to remove residual grafoil. The final finishing was completed with a #500 diamond grinding wheel under the specified condition in accordance with ASTM standard C1161 (Ref. 7).

2.4 X-ray Diffraction

X-ray diffraction (XRD) patterns of the as-received desert sand, CMAS glass powder, hot pressed samples, and glass powder heat-treated at different temperatures were recorded at ambient temperature using a step scan procedure (0.02°/2 θ step, count time 0.4 s) on a Bruker D8 Advanced diffractometer equipped with a crystal monochromator employing copper K $_{\alpha}$ radiation.

2.5 Thermal Analysis

Simultaneous differential thermal analysis (DTA) and thermogravimetric analysis (TGA) were carried out using Netzsch STA 409 C system interfaced with a computerized data acquisition and analysis system at heating/cooling rates of 5 or 10 °C/minute in flowing air. The test samples were contained in alumina cups. Glass transition and crystallization peak maximum temperatures were obtained from the DTA scans. To evaluate crystallization kinetics of the glass, DTA scans were recorded at various heating rates of 2 to 40 °C/minute.

2.6 Dilatometry

Glass transition temperature, softening point and coefficient of thermal expansion (CTE) were measured on a 2.5 cm long hot pressed glass bar using a Netzsch differential dilatometer model 402-C interfaced with a computerized data acquisition and analysis system at a heating rate of 5 °C/minute in air. Alumina was used as the standard material.

2.7 Density, Elastic Modulus, Microhardness, and Indentation Fracture Toughness

Density was measured from the bulk mass and volume of the hot pressed disc. Young's modulus, shear modulus, and Poisson's ratio were determined at ambient temperature by the impulse excitation method defined in ASTM C 1259 (Ref. 8) using the hot pressed glass disc. The test setup records the natural frequency of the disc when excited mechanically in the desired mode. An Audio Technica ATM350 condenser microphone amplified with an M-Audio DMP preamplifier was used to acoustically detect and amplify the natural frequency. A computer system instrumented with National Instruments acoustic signal acquisition hardware and Sound & Vibration Toolset software was used to determine the natural frequency.

Vickers microhardness was evaluated at ambient temperature using hot pressed glass disc with polished surfaces in accordance with ASTM C 1327 (Ref. 9). A Zwick model 3212 Hardness Tester was used for the Vickers diamond indent application. The Zwick hardness tester incorporates a dampening mechanism used to lower the indenter which remains in full load contact with the specimen for 15 sec. Four different indentation loads of 1.96, 2.9, 4.9, and 9.8 N were used for each series of tests. An upper limit of 9.8 N (1 kg) load was set by the indent exhibiting the start of extreme spalling. A number of indentations were made on the polished specimen using each load. Indentation diagonal length (2a) and crack length (2c) were measured using the integral optical micrometer for each impression. Values of microhardness and fracture toughness were determined from indentation length and crack length as described earlier (Refs. 10 to 12).

3.0 Results and Discussion

3.1 Desert Sand

3.1.1 Phase Composition

The XRD pattern (Fig. 1) of the as-received desert sand showed the presence of SiO_2 (Quartz), $\text{CaSO}_4 \cdot 2\text{H}_2\text{O}$ (Gypsum), CaCO_3 (Calcite), $\text{NaAlSi}_3\text{O}_8$ (Albite), and Mg-Al silicate phases. Approximate composition of the desert sand was calculated to be 34 percent SiO_2 (Quartz), 41 percent $\text{CaSO}_4 \cdot 2\text{H}_2\text{O}$ (Gypsum), 11 percent CaCO_3 (Calcite), 7 percent $\text{NaAlSi}_3\text{O}_8$ (Albite), and 5 percent Mg-Al silicate phases from semi-quantitative analysis of XRD results.

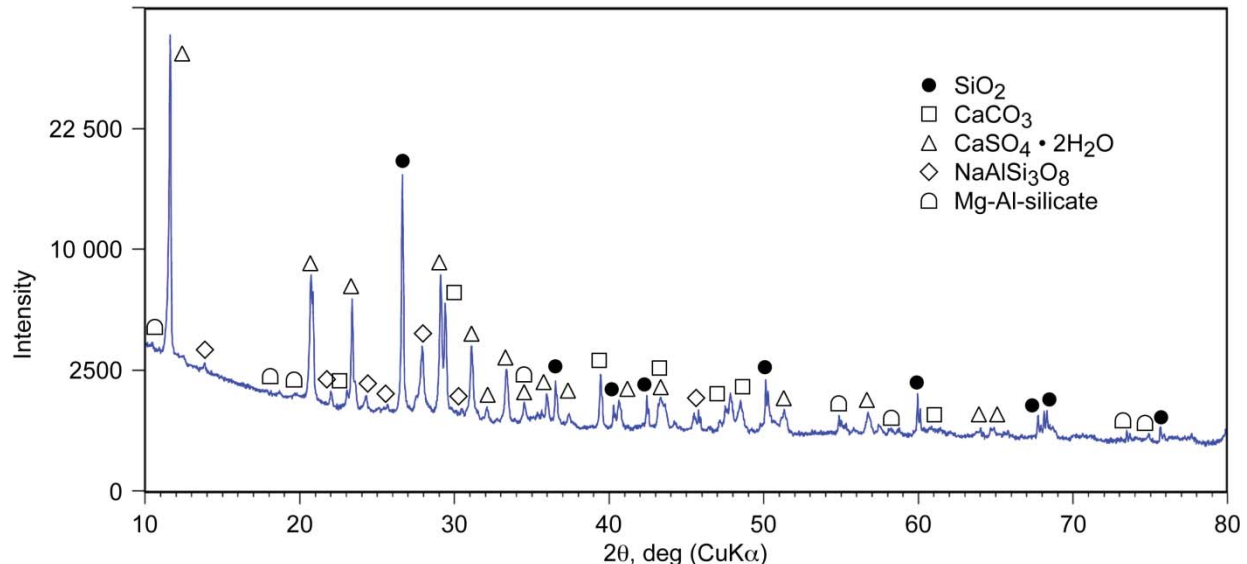


Figure 1.—X-ray diffraction of as-received desert sand from the Middle East showing the presence of $\text{CaSO}_4 \cdot 2\text{H}_2\text{O}$ (Gypsum), SiO_2 (Quartz), CaCO_3 (Calcite), $\text{NaAlSi}_3\text{O}_8$ (Albite), and Mg-Al Silicate phases.

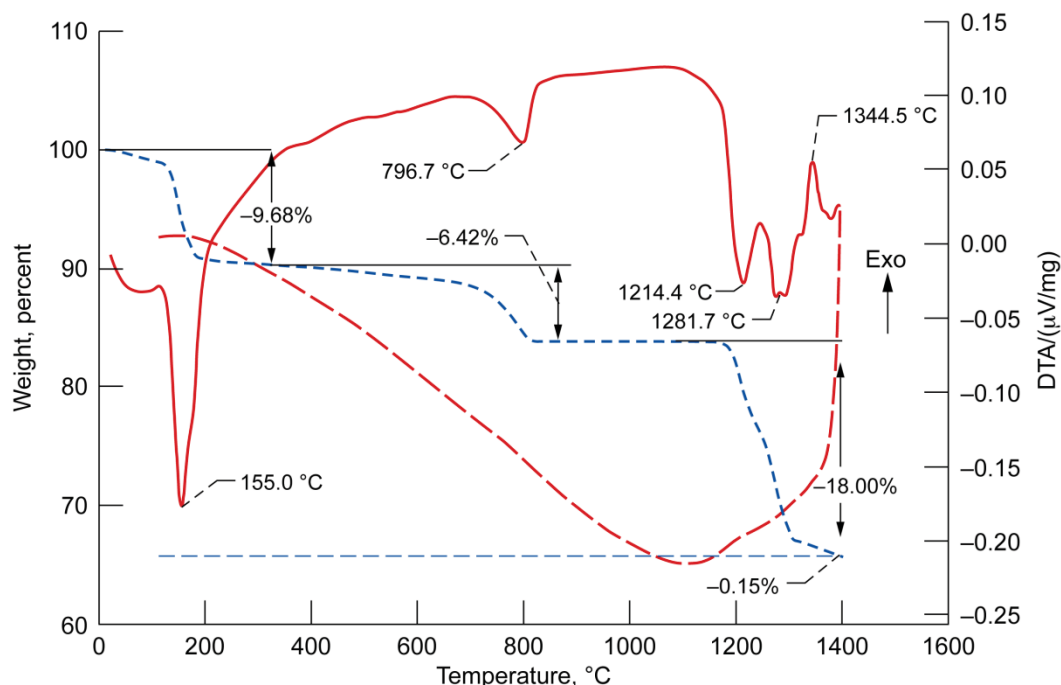


Figure 2.—Simultaneous DTA and TGA of as-received desert sand from the Middle East at a heating rate of 5 K/minute in air.

3.1.2 Thermal Stability

Simultaneous DTA/TGA scans of the as-received desert sand at a heating rate of 5 °C/minute in air from room temperature to 1420 °C are shown in Figure 2. Several thermal events are present. The endothermic peak in DTA at ~155 °C that is accompanied by a weight loss of ~9.68 percent is due to the dehydration of $\text{CaSO}_4 \cdot 2\text{H}_2\text{O}$ into CaSO_4 . The next endothermic DTA event at ~797 °C along with a weight loss of ~6.4 percent in TGA is ascribed to the decomposition reaction: $\text{CaCO}_3 \rightarrow \text{CaO} + \text{CO}_2$. Endothermic DTA peaks at 1214 and 1282 °C and corresponding weight loss of ~18 percent in TGA are probably due to the stepwise decomposition of CaSO_4 according to the reactions: $\text{CaSO}_4 \rightarrow \text{CaSO}_3 + \frac{1}{2} \text{O}_2$ followed by $\text{CaSO}_3 \rightarrow \text{CaO} + \text{SO}_2$. The exothermic peak at 1344 °C may be due to the formation of CaSiO_3 and/or $\text{CaAl}_2\text{Si}_2\text{O}_8$ phases via solid state reaction(s) between the constituents.

3.2 Glass

3.2.1 Composition

From inductively coupled plasma-atomic emission spectrometry (ICP-AES), chemical composition of the CMAS glass powder was analyzed to be 25.2CaO-2.6MgO-8.2Al₂O₃-59.8SiO₂-1.6Fe₂O₃-1.5K₂O (weight %) or 27.8CaO-4MgO-5Al₂O₃-61.6SiO₂-0.6Fe₂O₃-1K₂O (mole %). Composition of the desert sand glass of the current study is richer in silica but contains lower amounts of CaO, MgO, and Al₂O₃ than the composition 35CaO-10MgO-7Al₂O₃-48SiO₂ (mole %) of the synthesized model CMAS used by other researchers (Refs. 1 to 4).

3.2.2 Crystallization

Simultaneous DTA/TGA scans of the CMAS glass powder recorded at a heating rate of 10 °C/minute in air are given in Figure 3. The DTA shows a glass transition inflection at 734 °C and a couple of exothermic peaks at 878 and 982 °C due to crystallization of glass. The crystallization onset temperature, T_x , for this glass is found to be ~880 °C from the DTA curve. No thermal event is observed during the cooling cycle. A large value of 146 °C for ($T_x - T_g$) indicates this glass to be highly stable.

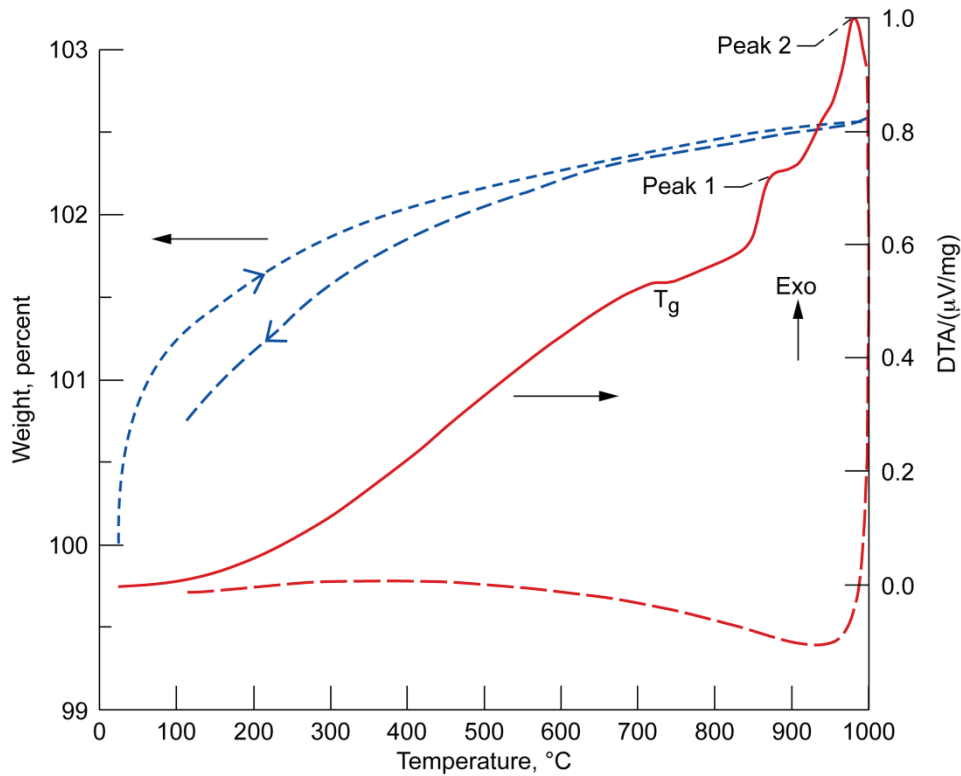


Figure 3.—Simultaneous DTA and TGA of sand CMAS glass powder at a heating rate of 10 K/minute in air.

To evaluate crystallization kinetics of the CMAS glass, DTA scans were recorded at various heating rates of 2 to 40 K/minute. A typical DTA scan recorded at a heating rate of 20 K/minute from room temperature to 1100 °C in air is shown in Figure 4. Values of peak maximum temperatures (T_p) for the two crystallization peaks at various scan rates are given in Table 1. Duplicate DTA runs were made at the scan rate of 5 K/minute. Values of T_{p1} and T_{p2} for the two runs at heating rate of 5 K/minute in Table 1 indicate very good reproducibility. Values of T_p are seen to increase with increase in heating rate. The crystallization peak maximum in the DTA or DSC scans corresponds to the temperature at which the rate of transformation of the viscous liquid into crystals becomes maximum. When the crystalline phase has the same composition as the liquid, the transformation rate will depend on the density of crystallization sites. However, when the composition of the crystalline phase is different from that of the liquid, as in the present case, the rate of transformation will be controlled by the rate of diffusion through the viscous liquid and the number of crystallization sites to which diffusion can occur. If the number of nucleation sites is increased, e.g., by using slower heating rates, the peak maximum will occur at a temperature at which the melt viscosity is higher, i.e., at a lower temperature. This explains the increase in T_p with the heating rate (Table 1) observed in the present study.

It has been shown earlier that the temperature T_p of the crystallization peak changes with heating rate θ according to the relation (Refs. 13 to 18):

$$\ln(T_p^2/\theta) = \ln(E_c/R\nu) + E_c/RT_p \quad (1)$$

where E_c is the effective overall activation energy for the crystallization process, ν is an effective frequency factor which is a measure of the probability that a molecule having energy E participates in the transformation, and R is the gas constant. According to Equation (1), a plot of $\ln(T_p^2/\theta)$ versus $1/T_p$ should be linear with a slope of E_c/R and an intercept $[\ln(E_c/R) - \ln \nu]$.

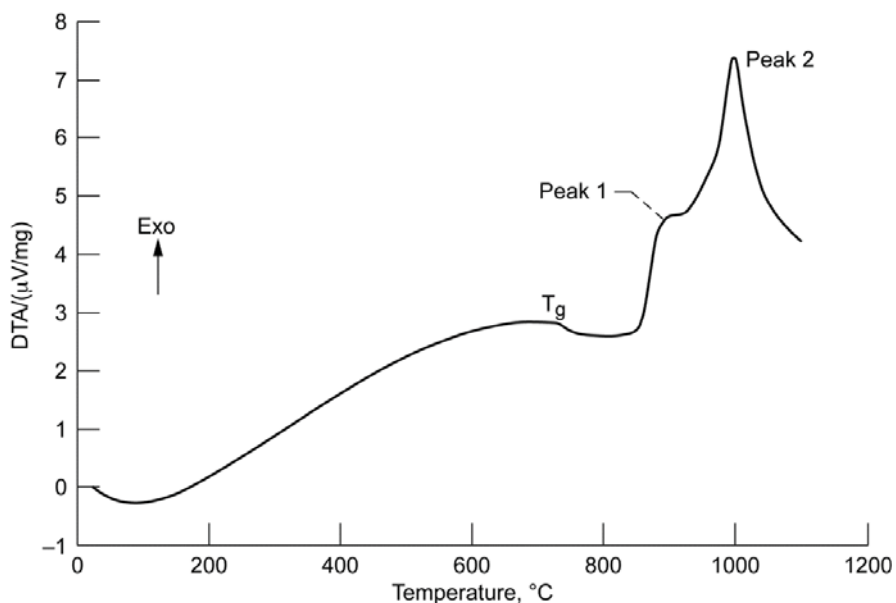


Figure 4.—DTA of desert sand CMAS glass powder at a heating rate of 20 K/minute in air.

TABLE 1.—EFFECT OF HEATING RATE ON DTA CRYSTALLIZATION PEAK MAXIMUM TEMPERATURES (T_p) FOR DESERT SAND GLASS

Scan rate (K/min)	Peak 1 (T_{p1}) (K)	Peak 2 (T_{p2}) (K)
2	1121	1209.8
5	1136	1234.7
5	1136	1234.7
10	1148	1254.9
20	1172	1271.2
30	1188	1280.1
40	1196	1285.9

Plots of $\ln(T_p^2/\theta)$ versus $1/T_p$ for crystallization of the CMAS glass are shown in Figure 5. A linear plot indicates validity of the kinetic model of Bansal et al. (Refs. 13 to 18) and validity of the assumptions made in this model. Values of kinetic parameters E and ν obtained from linear least squares fitting of the experimental data are listed in Table 2. The crystallization activation energies of 403 and 483 kJ/mol for CMAS glass are in the same range as reported earlier for barium aluminosilicate (BAS) (Refs. 16 and 17) and magnesium aluminosilicate (MAS) (Ref. 19) glasses.

The XRD pattern of the glass powder is shown in Figure 6. It contains only a large halo indicating the glass powder to be amorphous, as expected. XRD patterns of CMAS glass powder heat treated at various temperatures from 700 to 980 °C for 10 h in air are presented in Figure 7. The results for the development of crystalline phases in the CMAS glass after heat treatments at different temperatures are summarized in Table 3. The glass powder remains amorphous at temperatures up to 850 °C. However, two very minor peaks are present in the XRD of glass heated at 850 °C indicating the initiation of crystallization of CaSiO_3 . Glass heated at 870 °C is mostly amorphous but contains small crystallization peaks due to the formation of minor amounts of $\text{Ca}_2\text{Mg}_{0.5}\text{AlSi}_{1.5}\text{O}_7$ as well as trace amount of CaSiO_3 phase. Strong crystallization peaks are observed in the XRD patterns of glass heated at 900 or 980 °C. Glass heated at 900 °C shows the formation of $\text{Ca}_2\text{Mg}_{0.5}\text{AlSi}_{1.5}\text{O}_7$ as major phase and CaSiO_3 minor crystalline phase whereas CaSiO_3 is the major crystalline phase and Ca-Mg-Al silicate minor phase in the glass after heating at 980 °C. X-ray diffraction pattern from the surface of a glass disc hot pressed at 800 °C is shown in Figure 6. The sample is amorphous. The two low intensity peaks are from the presence of residual grafoil on the sample surface.

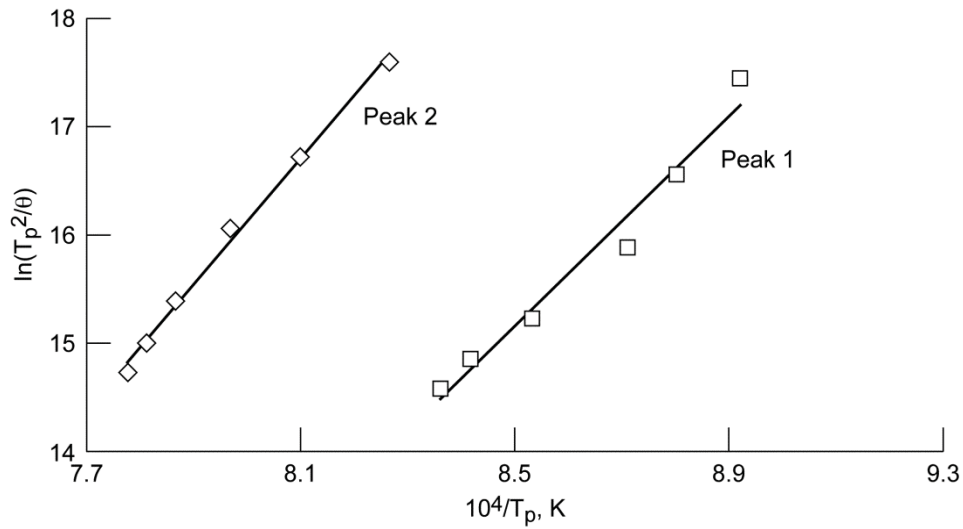
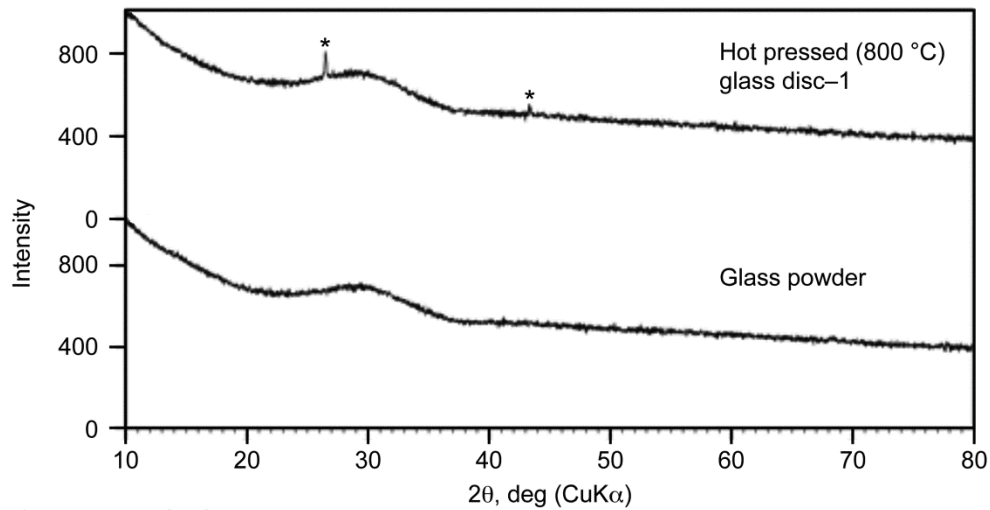


Figure 5.—Plots of $\ln(T_p^2/\theta)$ versus reciprocal of peak temperature for the two crystallization exotherms for desert sand CMAS glass powder.

TABLE 2.—KINETIC PARAMETERS FOR CRYSTALLIZATION OF DESERT SAND GLASS

Crystallization process	Activation energy, E_c (kJ/mol)	Frequency factor, ν (sec^{-1})
Peak 1	403	9.5×10^{15}
Peak 2	483	9.5×10^{17}



*Residual grafoil from hot pressing

Figure 6.—X-ray diffraction of desert sand CMAS glass powder and glass disc hot pressed at 800 °C for 10 min under 2.5 ksi in vacuum.

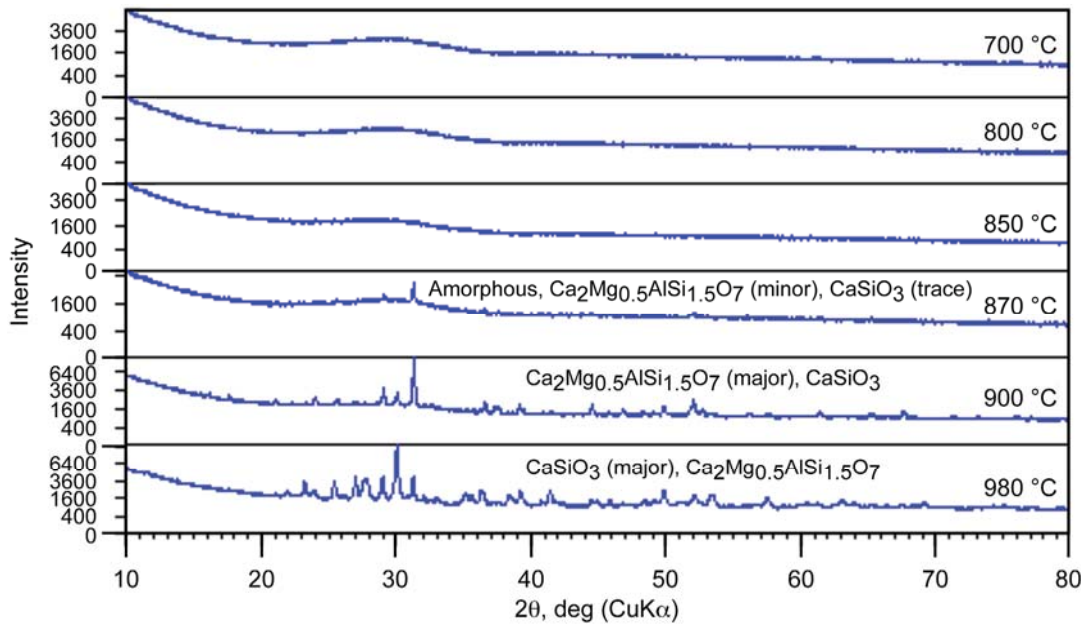


Figure 7.—X-ray diffraction of desert sand CMAS glass powder heat treated at various temperatures for 10 h in air.

TABLE 3.—DEVELOPMENT OF CRYSTALLINE PHASES IN DESERT SAND GLASS AFTER HEAT TREATMENTS AT VARIOUS TEMPERATURES FOR 10 h IN AIR

Sample	Temperature (°C)	Phases from XRD
SG-700	700	Amorphous
SG-800	800	Amorphous
SG-850	850	Amorphous
SG-870	870	Ca ₂ Mg _{0.5} AlSi _{1.5} O ₇ , CaSiO ₃
SG-900	900	Ca ₂ Mg _{0.5} AlSi _{1.5} O ₇ , CaSiO ₃
SG-980	980	CaSiO ₃ , Ca ₂ Mg _{0.5} AlSi _{1.5} O ₇

3.2.3 Dilatometry

Dilatometric thermal expansion curve for a hot pressed one inch long glass bar, measured from room temperature to 820 °C at a scan rate of 5 °C per minute, is shown in Figure 8. This shows a glass transition temperature (T_g) of 706 °C and dilatometric softening point (T_d) of 764 °C. The average linear coefficient of thermal expansion (CTE), α , was calculated to be $9.8 \times 10^{-6}/^\circ\text{C}$ in the temperature range from 25 to 700 °C.

3.2.4 Temperature Dependence of Glass Viscosity

Temperature dependence of glass viscosity (η) is expressed by the Vogel-Fulcher-Tamman (VFT) Equation (20):

$$\log \eta = A + B/(T-T_0) \quad (2)$$

where A, B, and T_0 are constants. Melting point T_m of glass is estimated from Bemann Equation (21):

$$T_g/T_m = 2/3 \quad (3)$$

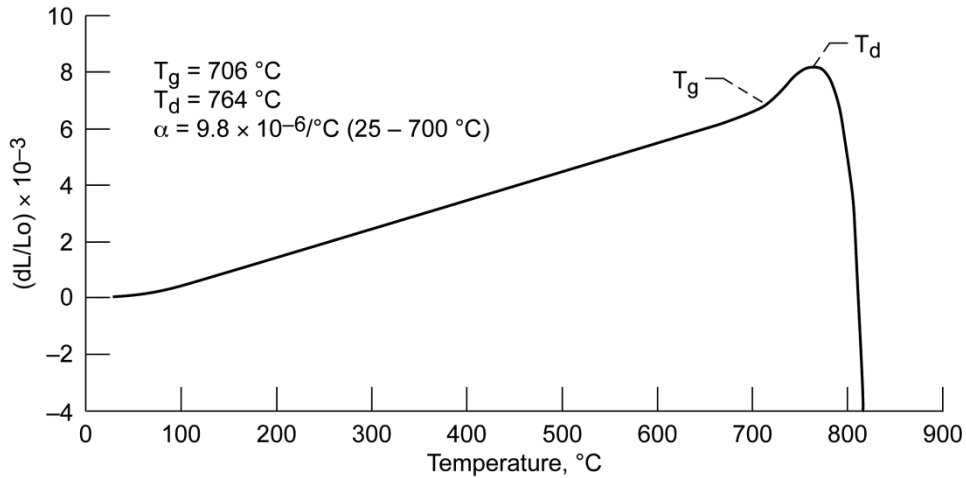


Figure 8.—Dilatometric thermal expansion scan of hot pressed desert sand CMAS glass at a heating rate of 5 °C/minute in air.

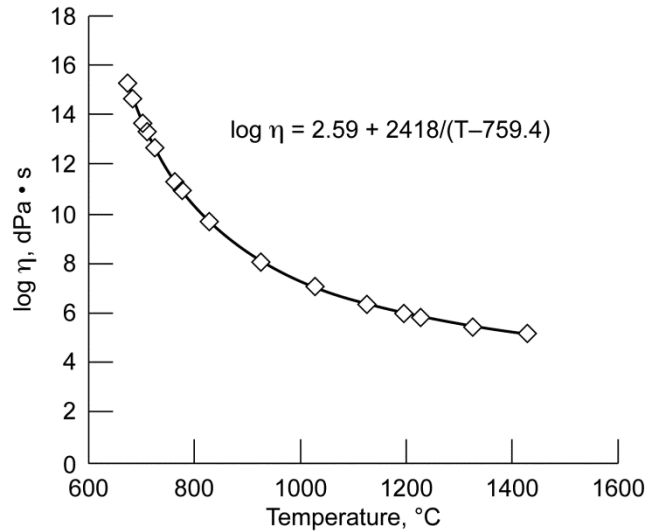


Figure 9.—Temperature dependence of viscosity of desert sand CMAS glass.

For silicate glasses, a number of specific viscosity values have been assigned as reference points corresponding to various temperatures. For silicate glasses, viscosity values at reference temperatures T_g , T_d , and T_m are designated as $10^{13.6}$, $10^{11.3}$, and 10^6 dPaS, respectively (Ref. 22). For the sand glass of the present study, values of T_g , T_d , and T_m are 979, 1037, and 1468.5 K. Values of constants A , B , and T_0 of VFT Equation (1) are determined from three equations by substituting η values corresponding to T_g , T_d , and T_m in Equation (2). For sand glass, values of these constants are calculated to be: $A = 2.6$ kPa.s, $B = 2418$ kPa.s.K, and $T_0 = 759$ K.

The VFT equation for the desert sand glass becomes:

$$\log \eta = 2.6 + 2418/(T-759) \quad (4)$$

Temperature dependence of viscosity of the desert sand glass is shown in Figure 9.

3.2.5 Density, Elastic Modulus, Microhardness, and Indentation Fracture Toughness

Bulk density of CMAS glass was determined to be 2.69 g/cm³ from weight and volume measurements. Values of Young's modulus (E), Shear modulus (G), and Poisson's ratio (σ) were measured to be 92.3 GPa, 36 GPa, and 0.28, respectively.

For Vickers microhardness measurements, a number of indentations were made on the surface of a hot pressed polished specimen using indentation loads of 1.96, 2.9, 4.9, and 9.8 N. Typical indentations on the glass specimen at various loads are shown in Figure 10. An upper limit of 9.8 N (1 kg) load was set by the indent exhibiting the start of extreme spalling. Indentation diagonal length (2a) and crack length (2c) were measured for each impression as shown in Figure 11. Results for an indentation were not included if value of c/a was less than 2.3 or if crack branching was present. Vickers microhardness was calculated using the equation:

$$H_v = 1.854 [P/(2a)^2] \quad (5)$$

where H_v is the Vickers microhardness in Pascal, P is the applied load in Newton, and 2a is the indent diagonal length in meter. Values of H_v at various loads are shown in Figure 12 and Table 4. Average value of H_v for the desert sand glass was found to be 6.3±0.4 GPa. This value of Vickers microhardness for desert sand glass falls in the same range as found for other silicate glasses.

A number of mathematical equations are available for determination of indentation fracture toughness (Refs. 23 to 27). Miyoshi et al. (Ref. 23) provided the relation:

$$K_c = 0.0264 E^{0.5} P^{0.5} a/c^{-1.5} \quad (6)$$

where K_c is the indentation fracture toughness in MPa.m^{1/2}, E is the Young's modulus in GPa, P is the indentation load in Newton, a is the half indent length in meter, and c is the half crack length in meter. Marshall and Evans (Ref. 24) reported the following relation:

$$K_c = 0.036 E^{0.4} P^{0.6} a^{0.8} c^{-1.5} \quad (7)$$

for evaluation of K_c . According to Anstis et al. (Ref. 25), K_c may be obtained from the equation:

$$K_c = \beta P (E/H_v)^{1/2} c^{-1.5} \quad (8)$$

where β is an empirical constant. Based on a fit to experimental data using independent fracture toughness measurements, Anstis et al. (Ref. 25) determined the value of β as 0.016±0.004. Values of K_c evaluated at various indentation loads from Equation (6) of Miyoshi et al. are shown in Figure 13. Values of K_c determined using various Equations (6) to (8) are listed in Table 4 which are found to be in good agreement with each other. For desert sand glass an average value of indentation fracture toughness was found to be 0.75±0.15 MPa.m^{1/2} which is typical as found for other silicate glasses. It will be interesting to compare these values with those obtained from the single edge V-notch beam (SEVNB) method.

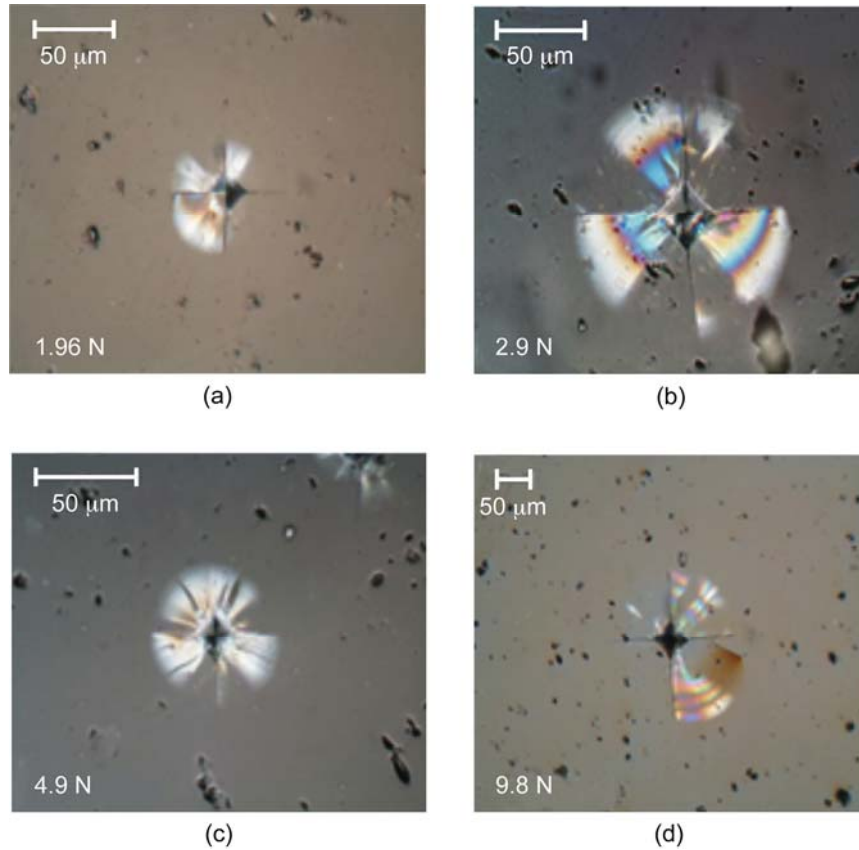


Figure 10.—Optical micrographs showing Vickers indentations on CMAS glass at applied loads of (a) 1.96 N, (b) 2.9 N, (c) 4.9 N, and (d) 9.8 N.

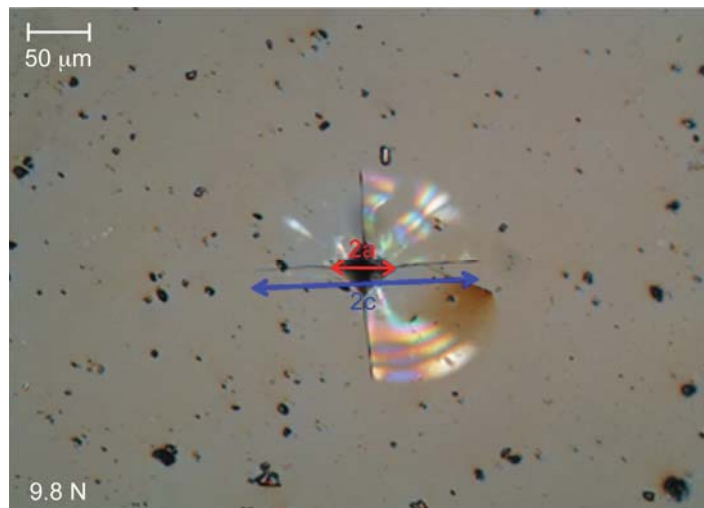


Figure 11.—Vickers indentation on CMAS glass at an applied load of 9.8 N showing indentation diagonal length ($2a$) and crack length ($2c$).

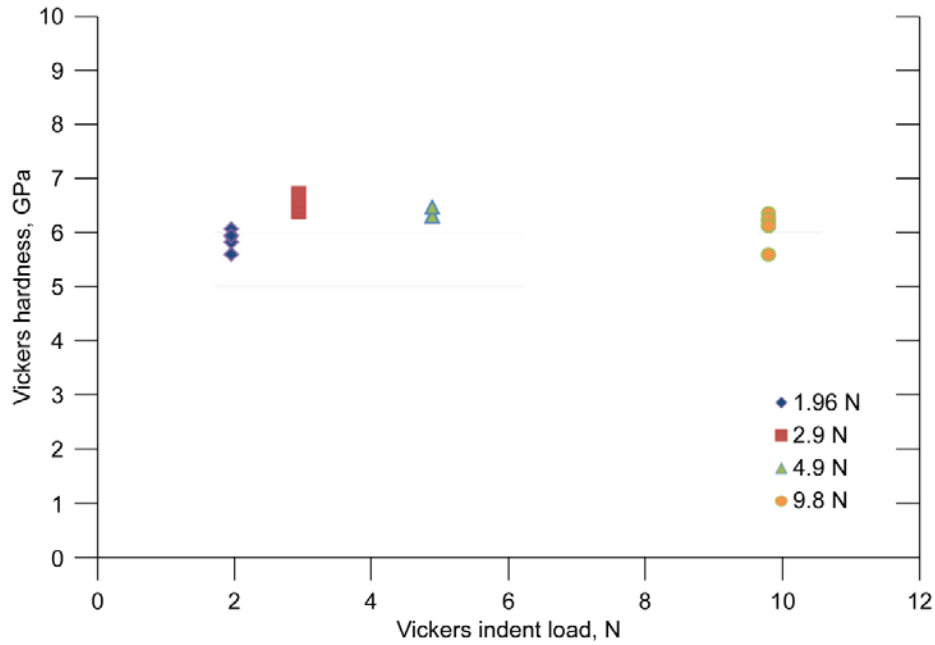


Figure 12.—Values of Vickers microhardness for desert sand CMAS glass at various indentation loads.

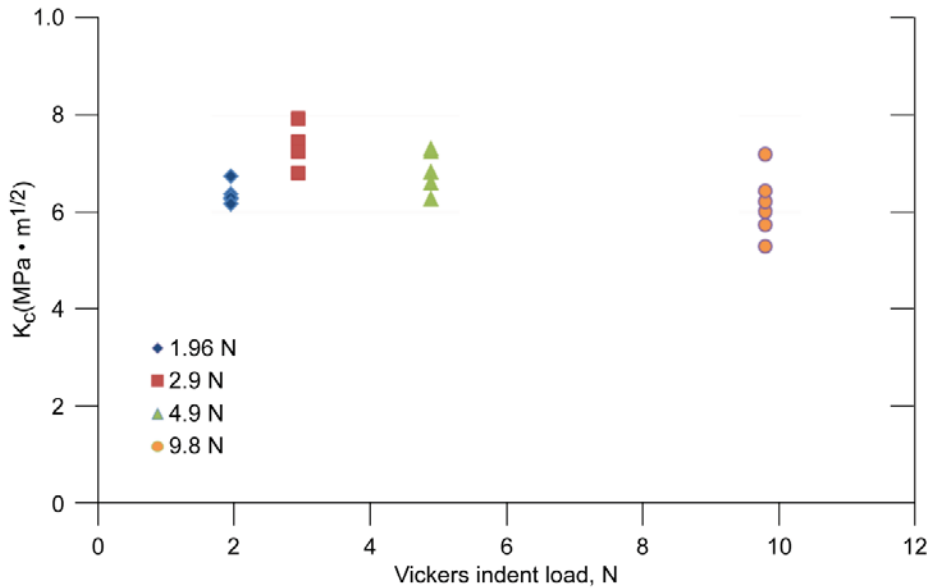


Figure 13.—Values of indentation fracture toughness evaluated using equation of Miyoshi et al. (Ref. 23) at various indentation loads for desert sand CMAS glass.

TABLE 4.—VICKERS HARDNESS AND INDENTATION FRACTURE TOUGHNESS OF DESERT SAND GLASS

Indent load (N)	Crack length (2c)/Indent length (2a)	Vickers hardness, H _v (GPa)	Indentation fracture toughness, K _c (MPa·m ^{1/2}), from various equations		
			Eq. (6) Miyoshi et al.	Eq. (7) Marshall & Evans	Eq. (8) Anstis et al.
1.96	2.9	5.9±0.1	0.7	0.7	0.6
2.94	2.8±0.1	6.6±0.1	0.8	0.9	0.7
4.9	3.2±0.1	6.4±0.1	0.75±0.05	0.8±0.1	0.65±0.05
9.8	3.8±0.2	6.2±0.1	0.65±0.05	0.7±0.1	0.6±0.1

4.0 Summary and Conclusions

As-received desert sand from the Middle east consisted of quartz (SiO_2), calcite (CaCO_3), gypsum ($\text{CaSO}_4 \cdot 2\text{H}_2\text{O}$) and $\text{NaAlSi}_3\text{O}_8$ phases and showed weight loss of ~35 percent due to decomposition of CaCO_3 and $\text{CaSO}_4 \cdot 2\text{H}_2\text{O}$ when heated to 1400 °C. Chemical composition of the glass, obtained by melting of desert sand at ~1500 °C, was analyzed to be $27.8\text{CaO}-4\text{MgO}-5\text{Al}_2\text{O}_3-61.6\text{SiO}_2-0.6\text{Fe}_2\text{O}_3-1\text{K}_2\text{O}$ (mole %) using inductively coupled plasma-atomic emission spectrometry. The glass remained amorphous after heat treating at 850 °C for 10 hr but crystallized into CaSiO_3 and Ca-Mg-Al silicate phases at 900 °C or higher temperatures. Various physical, thermal and mechanical properties of the glass have been evaluated. The glass showed bulk density 2.69 g/cm³, Young's modulus 92 GPa, Shear modulus 36 GPa, Poisson's ratio 0.28, dilatometric glass transition temperature (T_g) 706 °C, softening point (T_d) 764 °C, Vickers microhardness 6.3 ± 0.4 GPa, indentation fracture toughness 0.75 ± 0.15 MPa.m^{1/2}, and coefficient of thermal expansion (CTE) $9.8 \times 10^{-6}/^\circ\text{C}$ in the temperature range 25 to 700 °C. Temperature dependence of viscosity of the CMAS glass has been estimated from viscosity values at various reference points. Crystallization kinetics of the CMAS glass was also investigated by differential thermal analysis (DTA). Activation energies for crystallization of two different phases in the glass were calculated to be 403 and 483 kJ/mol, respectively.

5.0 Future Work

Future research will involve the determination of strength of desert sand glass in 4-point bend as well as its fracture toughness by single edge v-notch beam (SEVNB) method. Interactions of this CMAS glass will also be investigated with various environmental barrier coating (EBC) and thermal barrier coating (TBC) materials at elevated temperatures of 1200 to 1500 °C. Effects of sand glass exposures on stability of EBC and TBC coatings as well as SiC_f/SiC composites will also be studied.

References

1. K. M. Grant, S. Kramer, G. G. E. Seward, and C. G. Levi, Calcium-Magnesium Alumino-Silicate Interaction with Yttrium Monosilicate Environmental Barrier Coatings, *J. Am. Ceram. Soc.*, 93 [10], 3504-3511 (2010).
2. K. M. Grant, S. Kramer, J. P. A. Lofvander, and C. G. Levi, CMAS Degradation of Environmental Barrier Coatings, *Surface Coatings Technol.*, 202 [4-7], 653-657 (2007).
3. B. J. Harder, J. Ramirez-Rico, J. D. Almer, K. N. Lee, and K. T. Faber, Chemical and Mechanical Consequences of Environmental Barrier Coating Exposure to Calcium-Magnesium-Aluminosilicate, *J. Am. Ceram. Soc.*, 94 [S1], S178-S185 (2011).
4. S. Kramer, J. Yang, C. G. Levi, and C. A. Johnson, Thermochemical Interaction of Thermal Barrier Coatings with Molten $\text{CaO-MgO-Al}_2\text{O}_3\text{-SiO}_2$ (CMAS) Deposits, *J. Am. Ceram. Soc.*, 89 [10], 3167-3175 (2006).
5. X. Chen, Calcium-Magnesium-Alumina-Silicate (CMAS) Delamination Mechanisms in EB-PVD Thermal Barrier Coatings, *Surface Coatings Technol.*, 200 [11], 3418-3427 (2006).
6. C. Mercer, S. Faulhaber, A. G. Evans, and R. Darolia, A Delamination Mechanism for Thermal Barrier Coatings Subject to Calcium-Magnesium-Alumino-Silicate (CMAS) Infiltration, *Acta Mater.*, 53 [4], 1029-1039 (2005).
7. ASTM C 1161, Annual Book of ASTM Standards, Vol 15.01, ASTM, West Conshohocken, PA, 2006.
8. ASTM C1259, "Standard Test Method for Dynamic Young's Modulus, Shear Modulus, and Poisson's Ratio for Advanced Ceramics by Impulse Excitation of Vibration," Annual Book of ASTM Standards, Vol. 15.01, American Society for Testing and Materials, West Conshohocken, PA, 2001.

9. ASTM C 1327, Annual Book of ASTM Standards, Vol 15.01, ASTM, West Conshohocken, PA, 2006.
10. N. P. Bansal, J. B. Hurst, and S. R. Choi, Boron Nitride Nanotubes-Reinforced Glass Composites, *J. Am. Ceram. Soc.*, 89 [11], 3880390 (2006).
11. S. R. Choi, N. P. Bansal, and A. Garg, Mechanical and Microstructural Characterization of Boron Nitride Nanotubes-Reinforced SOFC Seal Glass Composite, *Mater. Sci. Eng. A*, 460-461, 509-515 (2007).
12. S. R. Choi and N. P. Bansal, Mechanical Properties of SOFC Seal Glass Composites, *Ceram. Eng. Sci. Proc.*, 26 [4], 275-283 (2005).
13. N. P. Bansal and R. H. Doremus, Determination of Reaction Kinetic Parameters from Variable Temperature DSC or DTA, *J. Thermal Anal.*, 29, 115 (1984).
14. N. P. Bansal, R. H. Doremus, A. J. Bruce, and C. T. Moynihan, Kinetics of Crystallization of ZrF_4 - BaF_2 - LaF_3 Glass by Differential Scanning Calorimetry, *J. Am. Ceram. Soc.*, 66 [4], 233 (1983).
15. N. P. Bansal, A. J. Bruce, R. H. Doremus, and C. T. Moynihan, The Influence of Glass Composition on the Crystal Growth Kinetics of Heavy Metal Fluoride Glasses, *J. Non-Cryst. Solids*, 70, 379 (1985).
16. N. P. Bansal and M. J. Hyatt, Crystallization Kinetics of Barium Aluminosilicate Glasses, *J. Mater. Res.*, 4, 1257 (1989).
17. M. J. Hyatt and N. P. Bansal, Crystal Growth Kinetics in $BaO \cdot Al_2O_3 \cdot 2SiO_2$ and $SrO \cdot Al_2O_3 \cdot 2SiO_2$ Glasses, *J. Mater. Sci.*, 31 [1], 172-184 (1996).
18. N. P. Bansal and E. A. Gamble, Crystallization Kinetics of a Solid Oxide Fuel Cell Seal Glass by Differential Thermal Analysis, *J. Power Sources*, 147 [1-2] 107-115 (2005).
19. D. Bahadur, N. Lahl, K. Singh, L. Singheiser, and K. Hilpert, Influence of Nucleating Agents on the Chemical Interaction of MgO - Al_2O_3 - SiO_2 - B_2O_3 Glass Sealants with Components of SOFCs, *J. Electrochem. Soc.*, 151[4], A558-A562 (2004).
20. A. K. Varshneya, Fundamental of Inorganic Glasses, Academic Press, New York, 1994, p. 188.
21. R. G. Beman and F. B. Cramer, Polymer characterization: A typical copolyamide system, *J. Polymer Sci.*, 21, 223-235 (1956).
22. N. P. Bansal and R. H. Doremus, Handbook of Glass Properties, Academic Press, New York, 1986.
23. T. Miyoshi, N. Sagawa and T. Sassa, Study on Fracture Toughness Evaluation for Structural Ceramics, *Trans. Jpn. Soc. Mech. Eng.*, 51A, 2487-2489 (1985).
24. D. B. Marshall and A. G. Evans, Reply to Comment on Elastic/Plastic Indentation Damage in Ceramics: The Median/Radial Crack System, *J. Am. Ceram. Soc.*, 64 [12], C182-C183 (1981).
25. G. R. Anstis, P. Chantikul, B. R. Lawn, and D. B. Marshall, A Critical Evaluation of Indentation Techniques for Measuring Fracture Toughness: I, Direct Crack Measurements, *J. Am. Ceram. Soc.*, 64 [9], 533-538 (1981).
26. G. D. Quinn, J. Salem, I. Bar-on, K. Cho, M. Foley, and H. Fang, Fracture Toughness of Advanced Ceramics at Room Temperature, *J. Res. Natl. Inst. Stand. Technol.*, 97, 579-607 (1992).
27. G. D. Quinn and R. C. Bradt, On the Vickers Indentation Fracture Toughness Test, *J. Am. Ceram. Soc.*, 90 [3], 673-680 (2007).

